PHILOSOPHICAL TRANSACTIONS A

rsta.royalsocietypublishing.org

Research

Cite this article: Pinchak M, Ombrello T, Carter C, Gutmark E, Katta V. 2015 The effects of hydrodynamic stretch on the flame propagation enhancement of ethylene by addition of ozone. *Phil. Trans. R. Soc. A* **373**: 20140339.
http://dx.doi.org/10.1098/rsta.2014.0339

Accepted: 5 May 2015

One contribution of 14 to a theme issue 'Physics and chemistry of plasma-assisted combustion'.

Subject Areas:
mechanical engineering, chemical physics, plasma physics

Keywords:
plasma, combustion, ozone, flame speed enhancement, Hencken flame, sub-atmospheric pressure

Author for correspondence:
Timothy Ombrello
e-mail: timothy.ombrello.1@us.af.mil

The effects of hydrodynamic stretch on the flame propagation enhancement of ethylene by addition of ozone

Matthew Pinchak[1], Timothy Ombrello[2], Campbell Carter[2], Ephraim Gutmark[1] and Viswanath Katta[3]

[1]Department of Aerospace Engineering, University of Cincinnati, Cincinnati, OH, USA
[2]Aerospace Systems Directorate, US Air Force Research Laboratory, Wright-Patterson Air Force Base, OH, USA
[3]Innovative Scientific Solutions, Inc., Dayton, OH, USA

The effect of O_3 on C_2H_4/synthetic-air flame propagation at sub-atmospheric pressure was investigated through detailed experiments and simulations. A Hencken burner provided an ideal platform to interrogate flame speed enhancement, producing a steady, laminar, nearly one-dimensional, minimally curved, weakly stretched, and nearly adiabatic flame that could be accurately compared with simulations. The experimental results showed enhancement of up to 7.5% in flame speed for 11 000 ppm of O_3 at stoichiometric conditions. Significantly, the axial stretch rate was also found to affect enhancement. Comparison of the flames for a given burner exit velocity resulted in the enhancement increasing almost 9% over the range of axial stretch rates that was investigated. Two-dimensional simulations agreed well with the experiments in terms of flame speed, as well as the trends of enhancement. Rate of production analysis showed that the primary pathway for O_3 consumption was through reaction with H, leading to early heat release and increased production of OH. Higher flame stretch rates resulted in increased flux through the $H + O_3$ reaction to provide increased enhancement, due to the thinning of the flame that accompanies higher stretch, and thus results in decreased distance for the H to diffuse before reacting with O_3.

THE ROYAL SOCIETY PUBLISHING

1. Introduction

The trend in modern combustion systems towards operation at high efficiencies with reduced emissions requires the development of innovative methods to both enhance and control increasingly complicated combustion processes. Several applications that encourage the development of new methods to enhance the combustion process are state-of-the-art gas turbine engines, which operate at ultra-lean equivalence ratios to minimize NO_x and particulate emissions, and supersonic combustion ramjets (scramjets), where adequate mixing of the fuel and oxidizer and complete combustion must occur within the order of milliseconds. Such technologies naturally approach the limits provided by more traditional combustion techniques. One way to overcome these limits is to enhance the flame propagation and stabilization properties in such environments.

In order to achieve successful flame propagation, flame stabilization and complete combustion, additional energy must be injected into the system to accelerate the fuel oxidation processes. The typical technique to enhance fuel reactivity is to deposit additional energy into the combustor by way of elevated temperatures or by the production of highly reactive species. One of the most promising methods to deposit energy into a reactive system is through the application of plasma. The injection of plasma has the benefits of providing on-demand and *in situ* energy addition. This means that the energy can be deposited directly into a flame front or into the reactants. Over the past several decades, the application of plasma to combustion systems has been shown to help reduce ignition delay time [1–6], enhance flame stabilization [7–9], increase the flame propagation speed [10–12] and reduce emissions [13,14]. Many of the studies have focused on non-thermal plasmas, which can be more effective than thermal plasmas in producing better species selectivity to enhance combustion [15–17].

The studies cited above rely on the plasma production of various short-lived oxygen- and nitrogen-containing species and can be complicated by the highly coupled plasma–flame interaction. Therefore, one avenue of effort has been to clearly define a combustion system and introduce specific plasma-produced species in an attempt to isolate the enhancement mechanisms [18–22]. One such plasma-produced species is ozone (O_3). Previous studies have shown that O_3 can enhance both flame propagation and stabilization [18–22], as well as used to control combustion processes in homogeneous charge compression ignition engines [23–25]. In addition, the production of plasma species such as O_3 is important due to the relevance that it can have in the practical application of the technology. This is because O_3 is easily produced and, due to its long lifetime at lower temperatures (4000 s at 300 K [26]), easily transported to the reaction zone. As such, plasma production of O_3 provides a means for energy to be coupled into a flow in one location and extracted in another with minimal energy loss.

While thermal enhancement through elevated temperatures is a well-known method to enhance the rate of fuel oxidation, it can be inefficient, whether from heat loss to hardware or because of having to increase all energy degrees of freedom in the reactive system. Kinetic enhancement, where energy is used to change reaction pathways by creating active species, is more selective, and therefore can be more efficient vis-à-vis the enhancement achieved. Ozone can enable kinetic enhancement of flames through the activation of reactions at lower temperatures, which in turn leads to early heat release. Indeed, O_3 has already been shown to increase flame speed for hydrocarbons such as methane (CH_4) [18–22] and propane (C_3H_8) [21,22]. Furthermore, the enhancement has been shown to be strongly dependent on the equivalence ratio, with lean and rich mixtures being enhanced more compared with the stoichiometric condition. While alkanes like CH_4 and C_3H_8 have been investigated, it is of interest to pursue other fuels with different chemical structure in order to understand whether the enhancement pathways are similar. As larger hydrocarbons can have different fuel decomposition pathways (thermal versus radical reactions) in the early portion of the flame, this understanding can help determine the dominant enhancement mechanism when O_3 is produced and interacts with such fuels.

Equally as important as the enhancement with different fuels is the influence of flame stretch. Most of the previous plasma-assisted combustion studies have not focused on detailed

measurements of how hydrodynamic flame stretch influences enhancement when specific plasma-produced species are present. When looking towards more realistic and practical applications, the effect of stretch is critical because it is nearly always present. Specifically for O_3, the effect of stretch may be more pronounced because of the possibility of different decomposition and reactive pathways in the early stages of the flame zone. As the enhancement by O_3 can rely on both O_3 decomposition as well as the direct reaction of O_3 with other species that are present in the early region of the flame, the upstream diffusion of species and their composition are critical to enhancement. Flame stretch, which influences the flame thickness, has the potential to change the relative distribution of species because of upstream diffusion within the preheat zone [27]. Therefore, O_3 enhancement can potentially have different coupling and enhancement mechanisms depending on the flame structure.

The goal of this study was to investigate the kinetic enhancement effects of O_3 on ethylene (C_2H_4)–air flame propagation, as well as the influence of hydrodynamic stretch on enhancement. Measurements of the flame propagation enhancement were accomplished using the laser diagnostic technique of particle image velocimetry (PIV), and the kinetic enhancement pathways as a function of flame stretch rates were identified through detailed numerical simulations.

2. Experimental set-up

A Hencken burner at sub-atmospheric pressure was used to measure flame speeds with and without O_3 addition over a range of stretch rates. The stretch rates were calculated from the slope of the velocity gradient immediately upstream of the minimum velocity and are therefore termed axial stretch rates [28]. The burner was chosen because it provides steady, laminar, nearly one-dimensional, minimally curved and nearly adiabatic premixed flames with weak stretch (10–100 s^{-1}) and sufficient lift-off height to interrogate flame speed with PIV [28].

(a) Burner platform

The experiments were performed using a Hencken burner (Technologies for Research Model RT1 × 1) inside a variable pressure chamber. At atmospheric pressures and above, the flame produced by a Hencken burner is fairly well known, where the fuel and oxidizer are separated until the burner exit, whereupon they mix and establish a flame with sufficient standoff to suppress heat loss to the burner. The flame is stabilized by propagating to a region of mixing as well as by a small amount of heat loss to the burner surface. While this flame is ideal for producing a nearly adiabatic flame, it is not ideal for flame speed measurements. This is because the flame is somewhat wrinkled from concentration and velocity gradients. When the flow velocity is increased beyond the laminar flame speed, the flame lifts off non-uniformly and easily blows off because of the weak stability mechanism. On the other hand, at sub-atmospheric pressure, because of increased diffusivity, the flame produced by a Hencken burner can be stabilized at significant lift-off heights [28]. These flames are steady, laminar, nearly one-dimensional, minimally curved and nearly adiabatic. Furthermore, because of the increased diffusivity at lower pressures, the flames are premixed even when the reactants exiting the burner are non-premixed.

Additionally, the Hencken flames at sub-atmospheric pressure are weakly stretched. Without the presence of the flame, the exit flow of the burner remains at a constant velocity with no axial or radial gradients. The presence of the flame causes the flow to diverge, establishing a velocity gradient where the flame can stabilize. Different burner exit velocities do not result in appreciable changes to the minimum velocity, which is equivalent to the flame speed. This indicates that the flame is in a dynamic balance with the local flow velocity, with the only difference in flame speed originating from stretch effects. Therefore, as the burner exit velocity is increased at a fixed equivalence ratio, the burning flux of the flame has to increase. The only way for the flame to accomplish this is by increasing its area, which in turn increases the amount of flow divergence. This produces higher stretch rates at the flame front, spanning an approximate range from 0 to

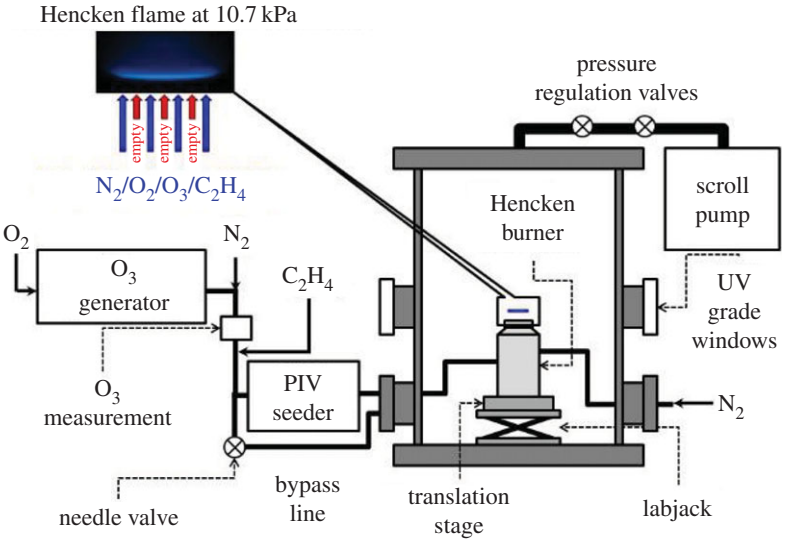

Figure 1. Schematic of variable pressure chamber and Hencken burner experimental set-up with inset photograph of flame at 10.7 kPa. (Online version in colour.)

$100\,s^{-1}$ [28]. The unique characteristics of the Hencken flame at sub-atmospheric pressure are vital to the discussions that will ensue throughout the remainder of this paper.

The chamber is cylindrical and constructed of electro-polished stainless steel with inside dimensions of 38.7 cm in diameter and 71.8 cm in height. A schematic of the experimental set-up is shown in figure 1. Ultra-high purity O_2 (99.999%) was sent to the O_3 generator, which was maintained at an internal gauge pressure of 69 kPa in order to produce the desired concentrations of O_3. Ultra-high purity gas was used to minimize the production of nitric oxide (NO) and any other reactive species, so that all of the enhancement could be attributed to reaction with O_3. The O_2/O_3 mixture was then mixed with N_2 to create synthetic air (21% O_2 in 79% N_2 by volume), after which the gas flowed to the absorption cell (used to quantify the O_3 concentration). Immediately downstream of the absorption cell, C_2H_4 (more than 99.5% purity) was added to the flow, creating a premixture at a fixed equivalence ratio upstream of the burner. Farther downstream, some of the gas flowed through a bypass directly to the chamber, while the remainder continued through the particle seeder for PIV and into the Hencken burner. The bypass line (with flow regulated by a needle valve) provided control of the flame lift-off height, and hence the axial stretch rate, by diverting some gas away from the burner. This allowed for constant flow rates through the mass flow controllers at a fixed equivalence ratio, allowing for changes to the flow to the Hencken burner while maintaining a constant pressure in the O_3 generator and in the chamber. The Hencken burner was therefore run in a 'premixed' mode, but the mixture was only sent through the oxidizer honeycomb and not through the fuel tubes in order to prevent clogging of the burner by particles from PIV seeding. The increased diffusivity at sub-atmospheric pressure mitigated all of the gradients prior to the flame, resulting in a premixed flame [24]. There are four ports for optical access through fused-silica windows located 90° apart from each other at half the height of the chamber. Additionally, there are four access ports for feedthroughs of gases, controls, etc. Sub-atmospheric pressures were achieved using a scroll pump and regulation valves and monitored using a capacitance manometer (accurate within ±0.05 kPa). The pressure in the chamber was maintained at 10.7 kPa for all experiments. The pressure was also monitored in the O_3 absorption cell to ensure accurate O_3 measurements. Additionally, temperatures at three locations in the chamber were recorded: at the bottom and top of the chamber, as well as at the exit of the Hencken burner. Mass flow controllers, calibrated using a dry piston flow calibrator (Bios Definer 220), metered the gas flows and provided accuracy within ±1% of the indicated flowrate.

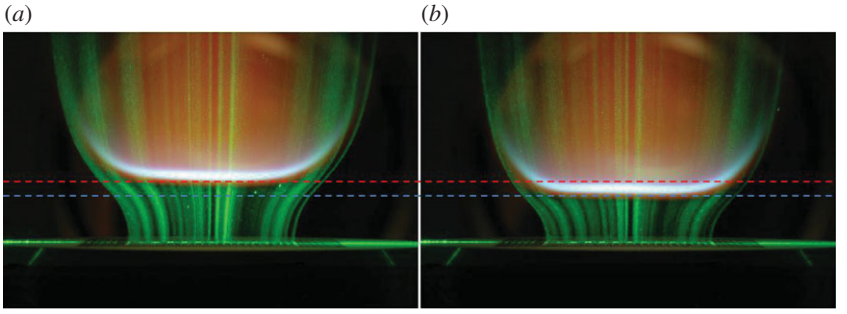

Figure 2. C_2H_4/synthetic-air Hencken flame seeded with TiO_2 particles for PIV measurements: 0 ppm O_3 (*a*) and 11 000 ppm O_3 (*b*). (Online version in colour.)

(b) Velocity measurement

PIV was used to measure the flame speeds with and without the presence of O_3, as well as the stretch rates from the velocity gradients upstream of the flame. To accomplish this, a New Wave Research Solo PIV dual Nd : YAG cavity system was used. The frequency-doubled 532 nm beams were sent through telescoping optics to produce a sheet collimated vertically at approximately 40 mm in height and focused in width after passing across the centre of the burner. This provided a vertical sheet above the burner of approximately 1 mm thickness. The mixture was seeded with less than 100 nm anatase titanium dioxide (TiO_2) particles, and the resulting scattering was imaged with a 1600 pixel by 1200 pixel interline-transfer, charge-coupled device camera (PCO 1600) using a 105 mm lens, with the f-stop set to f/11. Images were processed with the LaVision DaVis 8.0PIV software package. Care was taken to minimize reflections from the burner surface that would cause errors in the PIV correlations. Nevertheless, surface reflections corrupted the near-burner velocities (at distances less than or equal to 1 mm from the surface), therefore limiting the minimum axial stretch rates that could be resolved to approximately $40\,s^{-1}$. Long exposure images of both the unenhanced (without O_3) and enhanced (with O_3) seeded flames are shown in figure 2. For each condition, 150 image pairs were taken, with the timing difference between laser pulses set to $\Delta t = 90\,\mu s$. This Δt value was chosen based on the field of view and the expected velocities. Averages of velocity (for the 150 images) for several different widths across the middle of the flow were computed to determine the velocity profiles. A width of 8 mm was chosen to provide the most accurate representation of the velocities while remaining in the range of a linear radial velocity gradient [28]. Furthermore, at higher flame lift-off heights (more than 10 mm), entrainment from the N_2 curtain diluted the mixture and caused a decrease in the flame speed. Thus, flames with lift-off heights more than 10 mm were not used in this study.

(c) Experimental uncertainty analysis

The uncertainty in the velocity and stretch rate was dependent upon how the raw PIV data were processed. A convergence analysis was performed and led to small uncertainties of $1.22\,cm\,s^{-1}$ for the 0 ppm O_3 flames and $1.14\,cm\,s^{-1}$ for 11 000 ppm O_3 flames. This uncertainty is displayed with vertical error bars for the flame speeds when reporting the experimental results.

The stretch rate for a given dataset was determined by calculating the steepest velocity gradient just upstream of the minimum velocity. There are no rigorous guidelines to determine what range of data points should be used for this calculation, and therefore some subjectivity lies in the results. Generally, the stretch rates are reasonably constant over a significant portion of the curve before the minimum velocity point. In these cases, there is not a large concern of significant uncertainty in the stretch calculation. However, the inclusion or exclusion of just one or two data

points (approx. 0.2 mm per data point) has been observed to alter the stretch rate by as much as 4%. This error is displayed as the horizontal error bars reported in the experimental results. There are no error bars on the enhancement data as they are calculated from the trendlines of the flame speed data with and without O_3, and not as a one-to-one comparison.

(d) O_3 measurement

The O_3 concentration was measured using a single-pass, line-of-sight absorption cell with a 12.5 mm path length and fused-silica windows. An ultraviolet light-emitting diode (LED) with stable output provided radiation at the wavelengths covering the Hartley band of O_3, and an amplified photodiode detected transmission through the absorption cell. A bandpass filter was used to block ambient light and thus improve the fidelity of the measurement. The wavelength of 253.7 nm was used because O_3 has a peak absorption cross section there of 1.137×10^{-17} cm^2 (at 300 K) [29]. No other species present in the flow absorb at this wavelength. Therefore, the change in the transmittance with the O_3 generator on and off could be used to determine the O_3 number density (and hence concentration) through the Beer–Lambert law:

$$N_{\text{ozone}} = -\ln(I/I_0)/(\sigma_{\text{ozone}}L),$$

where N_{ozone} is the absolute number density of the absorbing species, O_3, I the intensity of light in the presence of O_3, I_0 the intensity of light without O_3, σ_{ozone} the absorption cross section of O_3 at the excitation wavelength (253.7 nm), and L the path length in the absorption cell (12.5 mm).

The intensity of light in the presence of O_3 was recorded during each test run using a digital oscilloscope (Teledyne LeCroy HDO6104). In addition, the output of the LED was monitored for fluctuations in output intensity using a second amplified photodiode. However, inevitable fluctuations in the O_3 generator and slight changes in pressure due to back-pressuring of the system by the seeder resulted in some fluctuation in O_3 concentrations of approximately $\pm$150 ppm (out of approx. 11 000 ppm) in the synthetic air. These small fluctuations were shown to be negligible through one-dimensional simulations of the flame speed enhancement under the conditions of the experiments.

As the O_3 measurement was performed upstream of the burner (as shown in figure 1), there was the potential for some of the O_3 to quench (i.e. react) before reaching the flame front. To verify that the internal surfaces of the particle seeder and tubing, as well as the fuel itself, did not quench the O_3 and that the amount measured was truly the amount at the flame front, a separate set-up was configured. Here, valves were installed such that the flow through the absorption cell could be changed quickly from the O_3/synthetic-air mixture directly from the O_3 generator to a flow path in which the particle seeder was placed between the O_3 generator and the O_3 absorption cell. A similar configuration was employed for the burner. In order to verify that the fuel did not quench the O_3, C_2H_4 was added to the O_3/synthetic-air mixture before it entered the absorption cell. The different set-ups showed no measureable difference in the O_3 concentration. Therefore, the internal surfaces of the particle seeder, tubing and burner, as well as the fuel, did not reduce the O_3 concentration. As the O_3 was produced upstream of the seeder, there was also the potential for the TiO_2 particles to quench some of the O_3. To confirm that there was minimal particle-induced quenching, a C_2H_4/synthetic-air flame representative of the ones used in the experiment was established without particle seeding. When the O_3 generator was turned on, the flame moved upstream due to the enhancement of the flame speed, and a long exposure photograph of the flame was taken. The seed was then introduced to the flow and a long exposure photograph taken again. As the flame lift-off height is very sensitive to changes in the flame speed, if the particles were quenching some of the O_3, the flame speed would decrease and the flame lift-off height would change. The results from the photographs showed no discernible difference in the flame lift-off height with O_3 and with and without particle seeding, indicating minimal particle-induced quenching of O_3.

3. Results and discussion

(a) Experimental results

As the Hencken flame at sub-atmospheric pressure is in a dynamic balance between the local flow velocity and the flame speed, any enhancement of the flame speed with the presence of O_3 results in the flame moving upstream. This is due to the flame (heat release) dictating the upstream velocity gradient, and hence stretch rate, where higher flame lift-off heights typically result in higher stretch rates [28]. PIV was performed to quantify the flame speed, stretch rates and enhancement by O_3, by finding the local minimum velocity and velocity gradient. Measurements were taken for 0 ppm O_3 and for approximately 11 000 ppm O_3, where 7.8% of the O_2 was converted to O_3. The conversion of some O_2 to O_3 inevitably resulted in a minor temperature rise. However, the dilution of the O_2/O_3 mixture with N_2 and heat loss to the flow surfaces in transit to the O_3 measurement cell and burner resulted in no appreciable rise in the gas temperature. The measurements were accomplished by varying the bypass in the system, which established the flame at certain lift-off heights. PIV was then performed without and with O_3 present. This resulted in a range of flames without and with O_3 across a range of flame lift-off heights and hence axial stretch rates. The results for a stoichiometric mixture are shown in figure 3. The flame speed increased with stretch rate, as would be expected for this stoichiometric C_2H_4/synthetic-air mixture, and the presence of O_3 clearly increased the flame speed.

(b) Simulations

In order to understand the mechanisms of enhancement, one-dimensional simulations were first performed using the PREMIX code from the CHEMKIN package [30]. The chemical kinetic mechanism of USC Mech II [31] was used because of successful comparisons to experiments in a previous study [28]. Twenty-six O_3 reactions from [19,20,22] were added to the mechanism and are shown in table 1. As mentioned above, it was confirmed experimentally that O_3 does not react with the fuel prior to the combustion zone. Gao *et al.* [32] showed that at higher pressures or at longer residence times, this is no longer the case, but at reduced pressures and the flow residence times in the current experiments, the reaction between the two is negligible. In addition, other works have noted that reactions between O_3 and saturated hydrocarbons such as CH_4 are quite slow at room temperature, and therefore the influence of O_3 on such fuels can be ignored [20]. Although the addition of reactions in the O_3 sub-mechanism does not consider synergistic effects, or how the addition of these reactions affects the rates of reactions present in the original mechanism, good agreement has been found between experimental results and the simulations [19,20,22].

From the one-dimensional simulations, flame speed enhancement with 11 000 ppm of O_3 was found to be over 11%, while the experimental enhancement was approximately 7%. This difference is partly due to the fact that the one-dimensional simulations fail to capture any stretch effects that would be present in these flames as the one-dimensional calculations are at zero stretch (figure 4). So while the kinetic processes would be captured, the comparison to the stretched flames in the experiments may not be suitable. Therefore, two-dimensional simulations were performed using the unsteady ignition and combustion with reactions (UNICORN) model [28,33–36]. UNICORN only requires the inflow conditions to determine the flame lift-off height and axial stretch rate.

The flame speed results for both the two-dimensional simulations and experiments are also shown in figure 4. There was excellent agreement between the measurements and simulations without the presence of O_3, further reinforcing the validity of the kinetic mechanism being used for these flames. With 11 000 ppm O_3, flame speeds derived from the simulations were greater than the measured values, but the trend of increased flame speed with stretch was captured.

To quantify the flame speed enhancement at each stretch rate, linear trendlines were fitted to the data with and without O_3 addition. The experimental results showed a fairly constant 7%

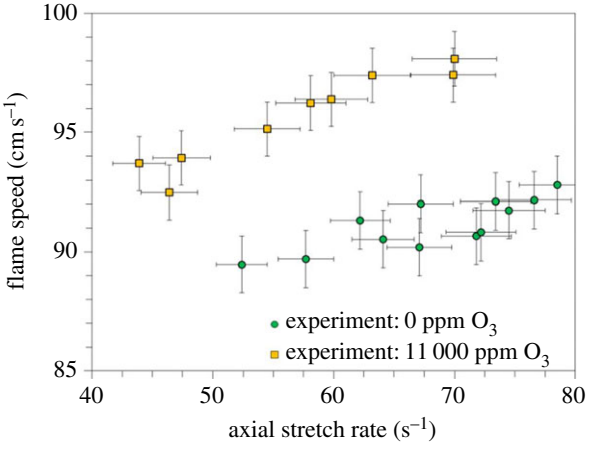

Figure 3. Experimental results of the flame speed with and without 11 000 ppm O_3 and enhancement versus axial stretch rate. (Online version in colour.)

increase in flame speed, with a slight trend of more enhancement at higher axial stretch rates (figure 4). This trendline compares the flame speed differences in unenhanced and enhanced flames with the same axial stretch rates. Another mode of comparison is to examine the variations in flame speed enhancement in flames that are stabilized in flow fields with identical burner exit velocities. This idea will be expanded upon later in the paper. A similar trend of near constant enhancement at each stretch rate is seen in the simulation data as well (figure 4). While the enhancement of flame speed was over-predicted, the trends were similar, indicating that the underlying mechanism of enhancement was correctly captured by the simulations and that the results could be used to analyse the mechanism in more detail.

As mentioned previously, it is the presence of the flame itself that produces both axial and radial velocity gradients in the Hencken burner flow field. In contrast to stagnation flames, the gradient disappears when there is no flame stabilized above the Hencken burner [28]. As the burner exit velocity increases, the radial velocity gradient also increases. This is because more flow is forced to slow to the laminar flame speed. The mechanism by which the flow does this is by spreading out radially, much like an increase in the cross-sectional area of a duct causes a decrease in the axial velocity of a constant-density fluid. As such, the increase in burner exit velocity results in a flame with a higher burning flux with a larger area and a higher stretch rate. This is depicted by Flame A in figure 5. If O_3 is then added to this flame, the flame speed increases and the flame finds a new dynamic balance closer to the burner exit; as the burning flux has not increased (the burner exit velocity is the same), the flame area remains the same and therefore forces more divergence of the flow. This is represented by Flame B in figure 5. Flames A and B both stabilize in a flow with an identical burner exit velocity, but due to the different flame propagation properties of the mixtures, they stabilize at positions with different local velocities and stretch rates. The flow fields are similar but distinct; the presence of the flames at different positions and with different flame propagation properties modifies the velocity field. This is shown by the different coloured streamlines in figure 5 and is also apparent in the pictures of figure 2. Therefore, in order to compare unenhanced and enhanced flames at the same stretch rate, the burner exit velocities for the two flames must be different.

Figure 4 describes the amount of enhancement for a given stretch rate. As explained in the preceding paragraph, the direct comparison of stretch rates means that the unenhanced and enhanced flames are stabilized in flows with different burner exit velocities. Due to the nuances of the flame structure, it seemed prudent to compare the unenhanced and enhanced flames at the same burner exit velocities. This comparison of the flames for a given burner exit velocity shows a significant increase in the dependence of flame speed enhancement on the axial stretch rate in both

Table 1. Ozone reaction sub-mechanism.

	reaction	A ($cm^3\ mol^{-1}\ s^{-1}$)	b	E ($kJ\ mol^{-1}$)	reference
1	$O_3 + O_2 \rightarrow O_2 + O + O_2$	1.54×10^{14}	0	96.5	[18]
2	$O_3 + O \rightarrow O_2 + O + O$	2.48×10^{15}	0	95.1	[18]
3	$O_3 + O_3 \rightarrow O_2 + O + O_3$	4.40×10^{14}	0	96.5	[18]
4	$O_3 + N_2 \rightarrow O_2 + O + N_2$	4.00×10^{14}	0	94.8	[18]
5	$O_2 + O + O_2 \rightarrow O_3 + O_2$	3.26×10^{19}	−2.1	0.0	[18]
6	$O_2 + O + N_2 \rightarrow O_3 + N_2$	1.60×10^{14}	−0.4	−5.8	[18]
7	$O_2 + O + O \rightarrow O_3 + O$	2.28×10^{15}	−0.5	−5.8	[18]
8	$O_2 + O + O_3 \rightarrow O_3 + O_3$	1.67×10^{15}	−0.5	−5.8	[18]
9	$O_2 + O_2 \rightarrow O + O + O_2$	9.80×10^{24}	−2.5	493.7	[18]
10	$O_2 + O \rightarrow O + O + O$	3.50×10^{25}	−2.5	493.7	[18]
11	$O_2 + O_3 \rightarrow O + O + O_3$	1.20×10^{19}	−1	493.7	[18]
12	$O_2 + H_2O \rightarrow O + O + H_2O$	1.20×10^{19}	−1	493.7	[18]
13	$O + O + O_2 \rightarrow O_2 + O_2$	1.50×10^{16}	−0.4	0.0	[18]
14	$O + O + N_2 \rightarrow O_2 + N_2$	6.00×10^{13}	0	−7.5	[18]
15	$O + O + O \rightarrow O_2 + O$	5.34×10^{16}	−0.4	0.0	[18]
16	$O + O + O_3 \rightarrow O_2 + O_3$	1.30×10^{14}	0	−7.5	[18]
17	$O_2 + O_2 \rightarrow O_3 + O$	1.20×10^{13}	0	419.8	[18]
18	$O_3 + O \rightarrow O_2 + O_2$	4.82×10^{12}	0	17.1	[18]
19	$O_3 + H \rightarrow OH + O_2$	8.43×10^{13}	0	3.9	[18]
20	$O_3 + H \rightarrow O + HO_2$	4.52×10^{11}	0	0.0	[16]
21	$O_2 + OH \rightarrow H + O_3$	4.40×10^{7}	1.4	329.2	[18]
22	$OH + O_3 \rightarrow HO_2 + O_2$	1.85×10^{11}	0	3.5	[18]
23	$O_3 + HO_2 \rightarrow OH + O_2 + O_2$	6.62×10^{9}	0	4.2	[18]
24	$O_3 + H_2O \rightarrow O_2 + H_2O_2$	6.62×10^{1}	0	0.0	[16]
25	$O_3 + CH_3 \rightarrow CH_3O + O_2$	5.83×10^{10}	0	0.0	[16]
26	$O_3 + H_2 \rightarrow OH + HO_2$	6.00×10^{10}	0	83.0	[15]

Arrhenius equation: $AT^b \exp(-E/RT)$

the experiments and two-dimensional simulations (figure 6). Though the maximum enhancement in figure 6 is similar to that shown in figure 4, the increase in stretch dependence is clearly evident, therefore warranting a more detailed investigation of the enhancement mechanism.

To accomplish this, rate-of-production analysis was performed using both the one- and two-dimensional simulations. It was found that there were two primary consumption pathways for O_3 in the early stages of the flame:

$$O_3 + H \rightarrow OH + O_2 \tag{3.1}$$

and

$$O_3 + N_2 \rightarrow O + O_2 + N_2 \tag{3.2}$$

with (3.1) being the dominant pathway. Vu *et al.* showed that for CH_4 at 101 kPa, the dominant pathway can change depending on the equivalence ratio, with (3.1) dominant at stoichiometric conditions but (3.2) dominant at lean and rich conditions [21]. Additionally, pressure effects

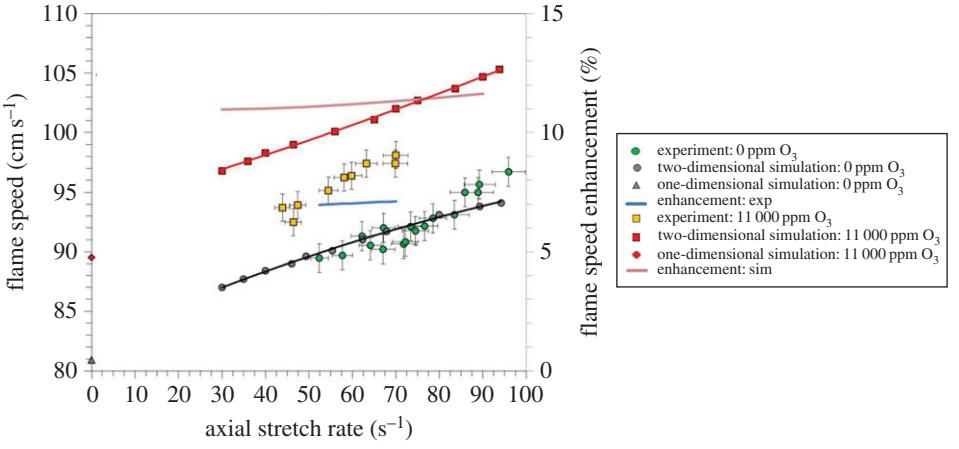

Figure 4. Experimental and numerical flame speed data and enhancement with and without 11 000 ppm O_3. (Online version in colour.)

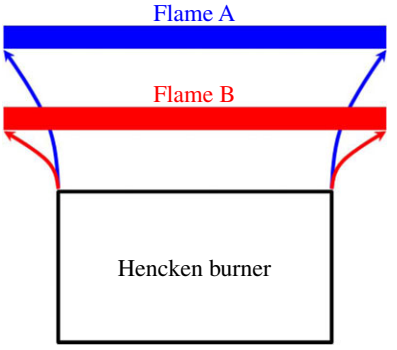

Figure 5. Schematic of unenhanced (Flame A) and enhanced (Flame B) flames stabilizing in similar flow fields, where the burner exit velocity remains constant. (Online version in colour.)

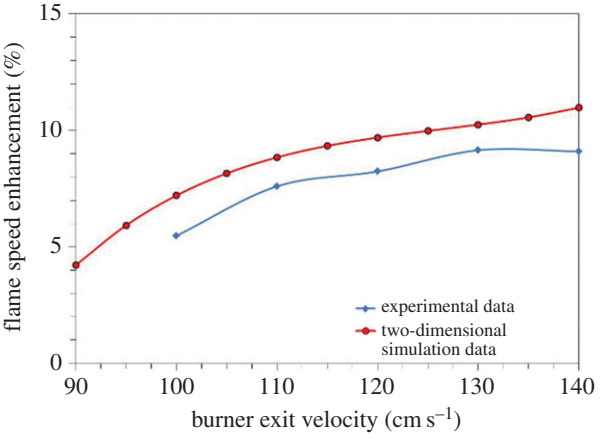

Figure 6. Flame speed enhancement with 11 000 ppm O_3 by comparing flames for the same burner exit velocity. (Online version in colour.)

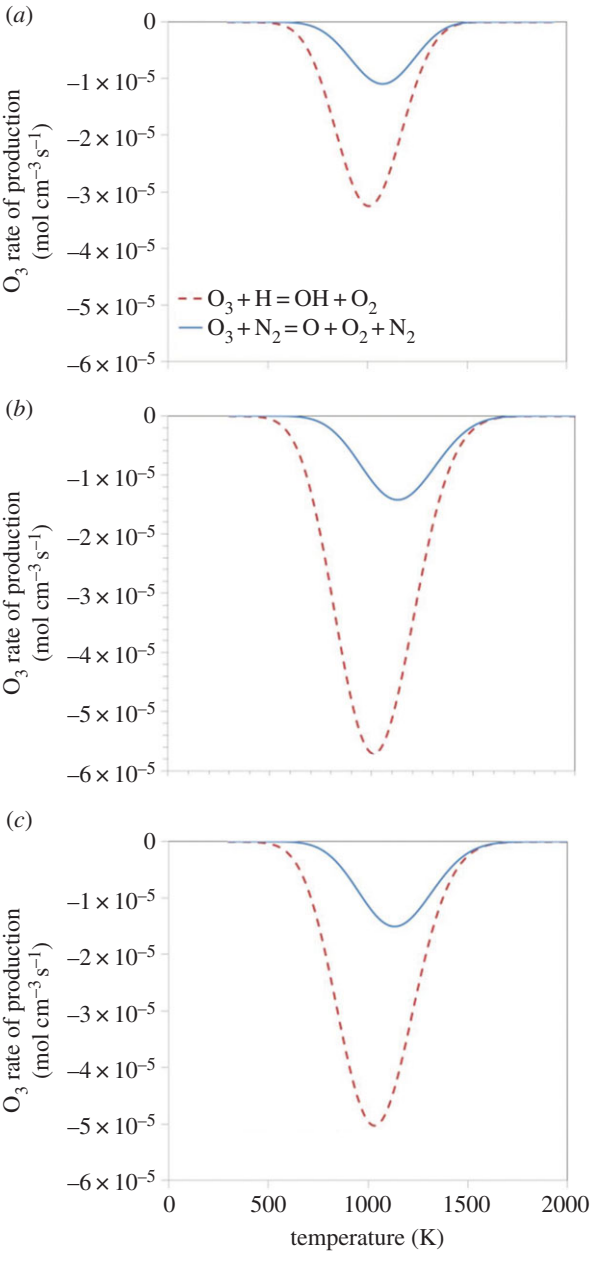

Figure 7. Primary consumption pathways of O_3 as a function of temperature through the flame at $\varphi = 0.7$ (*a*), 1 (*b*) and 1.3 (*c*) with addition of 11 000 ppm O_3 to C_2H_4/synthetic-air flames. (Online version in colour.)

have been observed for stoichiometric CH_4 where (3.2) becomes dominant over (3.1) above approximately 140 kPa [32]. Therefore, the major consumption pathways of O_3 with C_2H_4 at stoichiometric, lean and rich conditions at the 10.7 kPa used in the experiments are shown in figure 7. This is very different from what was observed for CH_4 [19,20] and C_3H_8 [22] in previous investigations, where the major O_3 consumption pathway was primarily O_3 decomposition. Interestingly, Vu *et al.* [21] and Gao *et al.* [32] also showed that (3.1) can in some cases inhibit flame speed enhancement as it is a chain propagation reaction (H to OH), whereas (3.2) is a chain initiation reaction (producing O radicals). However, for C_2H_4 under the conditions in these

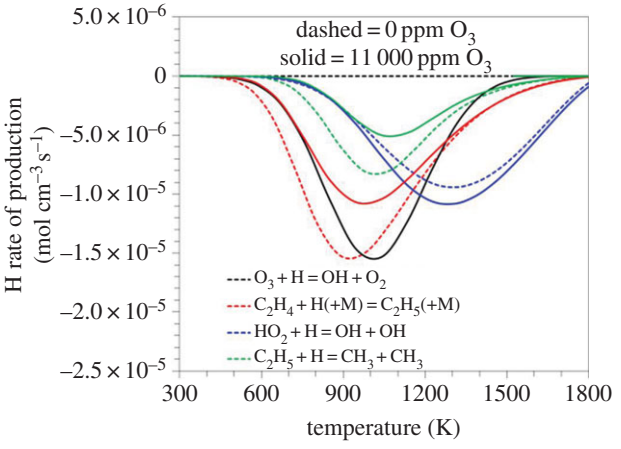

Figure 8. H rate of production with and without 11 000 ppm O_3. (Online version in colour.)

experiments, the simulation results show that this is not the case. This is because (3.1) competes with more detrimental pathways for H atoms, thereby reducing the flux through these inhibitive reactions.

For H consumption, (3.1) competed with

$$C_2H_4 + H(+M) \rightarrow C_2H_5(+M) \tag{3.3}$$

and in turn

$$C_2H_5 + H \rightarrow CH_3 + CH_3 \tag{3.4}$$

as shown in the rate of production of H in figure 8. With the decreased flux of H through (3.3) and (3.4), there was less production of C_2H_5 and CH_3, both of which are less reactive than C_2H_4. The figure also shows that the presence of O_3 encourages an increased flux of H with HO_2 to produce more OH, which in turn leads to more heat release.

As early heat release was determined to be one of the major contributors to flame speed enhancement with the presence of O_3, the contributions from each reaction were calculated and are shown in figure 9. While heat release from the reactions of HO_2, C_2H_3, HCO, CH_2O and C_2H_4 with OH increased, the most significant heat release early in the flame was clearly from (3.1). The figure shows that the amount of heat release from the reaction of HO_2 with OH substantially increases in the preheat zone. Without the early heat release from (3.1), HO_2 would be fairly unreactive in this region, where the additional OH from (3.1) is present. However, the increased temperatures in this part of the flame allow for a much greater flux of HO_2 through OH, which in turn results in additional early heat release. Furthermore, the increased flux through the reaction of C_2H_3 with O_2 not only thermally enhances the flame by increasing heat release in the preheat zone, but the increased production of HCO and CH_2O from this reaction further increases the amount of early heat release by the increased flux through the reaction of these species with O_2 and OH, respectively.

With the significant contribution of (3.1) to the flame speed enhancement through competition with other H consumption pathways, as well through heat release, it was considered that any uncertainty in this rate might explain the discrepancy in the enhancement between the experiments and simulations. To this end, a sensitivity analysis of this rate to the flame speed was performed using the uncertainty defined by the source of the rate [37]. With the rate of (3.1) changed to both the upper and lower values (dictated by the specified uncertainty), there was negligible change in the flame speed enhancement. Considering that (3.1) was the single most important reaction added in the O_3 sub-mechanism for C_2H_4 and its documented uncertainty is not, apparently, the source of the discrepancy in enhancement, it is reasonable to assume that

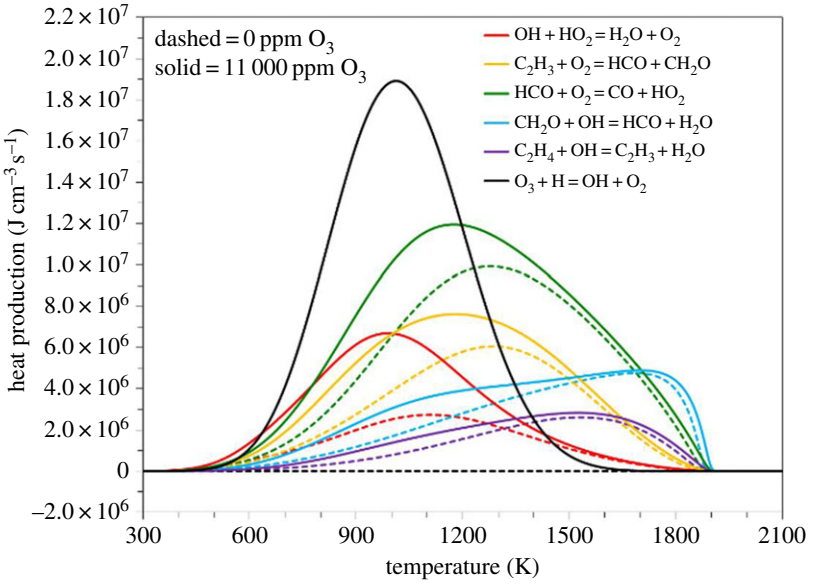

Figure 9. Change in heat release by O_3 addition. (Online version in colour.)

the source of the difference lies elsewhere and for now remains unknown. As more radicals were produced and more heat release occurred earlier in the flame with the presence of O_3, the reactions of radicals might be invoked at much lower temperatures than what the high temperature kinetic mechanism has been validated for. Therefore, the inclusion of low-temperature chemistry with special attention to the radical consumption pathways should be considered as the source of the enhancement discrepancy is unclear. This is a topic of current and future investigations.

One-dimensional simulations were performed to examine both lean and rich flame speed enhancement by O_3. Figure 10 shows that the speed and enhancement vary with equivalence ratio, with the minimum enhancement at near stoichiometric conditions. The result is expected because of the similar trends observed in previous investigations using other fuels [19]. The mechanism for the change as a function of equivalence ratio can be understood as a result of the lower chemical heat release of non-stoichiometric mixtures. Although the off-stoichiometric mixtures have lower laminar flame speeds than the stoichiometric case, the lower heat release makes them more responsive to a given amount of energy associated with the addition of O_3, which would be fixed for a given concentration of O_3. The higher enhancement of lean flames over rich flames can be explained by the lack of O and OH radicals in the flame region at rich conditions [22]. However, as enhancement was shown to be a strong function of the H concentration, it is possible that this behaviour is explained by H diffusion upstream, which varies with equivalence ratio.

While the mechanism of enhancement was found through the one-dimensional simulations, the increased enhancement with stretch remained unknown. As mentioned previously, the dependence of enhancement on flame stretch is most apparent when comparing unenhanced and enhanced flames with the same incoming velocities (burner exit velocities). This is equivalent to turning the O_3 generator on and off for a given flow condition (figure 6). Therefore, a rate-of-production analysis was performed using the two-dimensional simulation results with two exit velocities of 94 and 140 cm s^{-1}, which provided stretch rates of the unenhanced flame of approximately 10 and 100 s^{-1}, respectively. Examination of the primary O_3 reactions showed a sizeable change in (3.1) at higher stretch rates but little change in (3.2) (figure 11). Therefore, more heat was released early in the flame and more OH was produced, causing additional heat release through reactions with HO_2, C_2H_3, HCO, CH_2O and C_2H_4 (as shown in figure 9). Furthermore, there was less H present to react with C_2H_4 and C_2H_5 in (3.3) and (3.4), respectively.

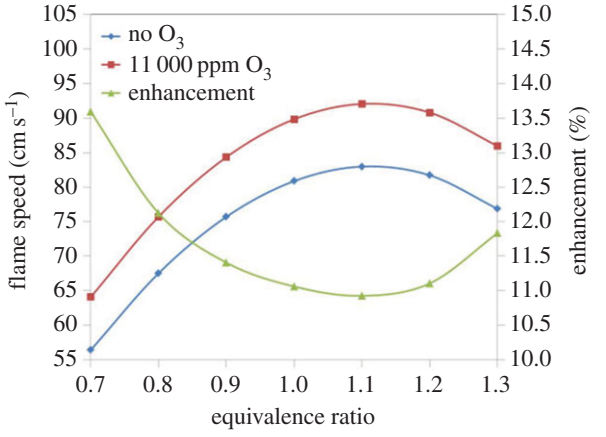

Figure 10. One-dimensional flame speed results with and without 11 000 ppm O_3 and enhancement as a function of equivalence ratio. (Online version in colour.)

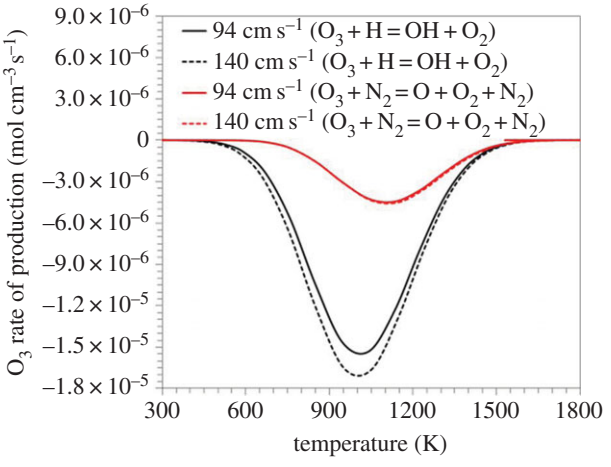

Figure 11. O_3 rate of production for different stretch rates. (Online version in colour.)

While the extra heat release early in the flame led to more flame speed enhancement at higher stretch rates, it is important to note that the O from O_3 decomposition (3.2) was still an important contributor to enhancement, but one that does not significantly vary with stretch. The increased importance of (3.1) at higher stretch rates can be explained by the change in flame structure. For a more highly stretched flame, the thickness of the flame decreases. Therefore, as the stretch rate is increased, the H that is produced at higher temperatures later in the flame does not have to diffuse as far upstream to react with O_3. This behaviour may be true for other radicals and therefore other reactions but may not be as pronounced as with H because of its high diffusivity.

4. Conclusion

Ozone was shown to enhance flame speed in stoichiometric C_2H_4/synthetic-air flames; the exact amount of enhancement with 11 000 ppm of O_3 depends on the axial stretch rate of the flame but was typically about 7% at moderate stretch rates. Numerical simulation results showed that the reaction of O_3 with H (forming OH) was the main contributor to flame speed enhancement by

directly releasing heat as well as introducing OH that in turn produced H_2O (and additional heat release through a secondary set of reactions). Furthermore, the reaction of O_3 with H competed with the other main H consumption reactions with C_2H_4 and C_2H_5 that led to the production of less reactive radicals that inhibited flame propagation. This is in contrast to the enhancement mechanism for CH_4 and C_3H_8, where the direct reaction of O_3 with H inhibits the flame speed. It is only the presence of the inhibitive reactions (3.3) and (3.4) in C_2H_4 combustion that allows the reaction of O_3 with H to have a beneficial effect on flame speed enhancement.

The importance of O_3 reacting with H led to an enhancement dependence on the axial stretch rate of the flame, with more heat release earlier in the flame zone at higher stretch rates. The result of increased enhancement with increased stretch, as well as at lean and rich equivalence ratios, has interesting implications as stretch and partial premixing (i.e. turbulence) are almost always present. Furthermore, the differences in the enhancement mechanism with C_2H_4 compared with other hydrocarbons suggest that other fuels with different fuel decomposition pathways may behave favourably to the presence of O_3. Also, many large hydrocarbon fuels can be cracked into small components during endothermic processes, indicating that O_3 addition might be used to control the flame propagation processes in a wide variety of combustion devices.

Authors' contributions. M.P. performed most of the experimental and computational work, as well as the majority of the analysis and drafting of the manuscript. T.O. conceived and designed the majority of the study, helped draft the manuscript, and advised on all aspects of the study. C.C. supported all of the diagnostic work, advised and helped draft the manuscript. E.G. helped advise the study. V.K. performed all of the two-dimensional simulations for the study. All authors gave final approval for publication.

Competing interests. The authors declare that they have no competing interests.

Funding. This work was supported by the Dayton Area Graduate Studies Institute.

References

1. Bozhenkov SA, Starikovskaia SM, Starikovskii AY. 2003 Nanosecond gas discharge ignition of H_2- and CH_4-containing mixtures. *Combust. Flame* **133**, 133–146. (doi:10.1016/S0010-2180(02)00564-3)
2. Lou G, Bao A, Nishihara M, Keshav S, Utkin YG, Rich JW, Lempert WR, Adamovich IV. 2007 Ignition of premixed hydrocarbon–air flows by repetitively pulsed, nanosecond pulse duration plasma. *Proc. Combust. Inst.* **31**, 3327–3334. (doi:10.1016/j.proci.2006.07.126)
3. Aleksandrov NL, Kindysheva SV, Kosarev IN, Starikovskaia SM, Starikovskii AY. 2009 Mechanism of ignition by non-equilibrium plasma. *Proc. Combust. Inst.* **32**, 205–212. (doi:10.1016/j.proci.2008.06.124)
4. Smirnov VV, Stelmakh OM, Fabelinsky VI, Kozlov DN, Starik AM, Titova NS. 2008 On the influence of electronically excited oxygen molecules on combustion of hydrogen–oxygen mixture *J. Phys. D Appl. Phys.* **41**, 192001. (doi:10.1088/0022-3727/41/19/192001)
5. Starik AM, Lukhovitskii BI, Titova NS. 2007 Mechanism of the initiation of combustion in $CH_4(C_2H_2)$/air/O_3 mixtures by laser excitation of the O_3 molecules. *Kinet. Catal.* **48**, 348–366. (doi:10.1134/S0023158407030032)
6. Lukhovitskii BI, Starik AM, Titova NS. 2005 Activation of chain processes in combustible mixtures by laser excitation of molecular vibrations of reactants. *Combust. Explos. Shock Waves* **41**, 386–394. (doi:10.1007/s10573-005-0047-6)
7. Kim W, Do H, Mungal MG, Cappelli MA. 2008 Optimal discharge placement in plasma-assisted combustion of a methane jet in cross flow. *Combust. Flame* **153**, 603–615. (doi:10.1016/j.combustflame.2007.11.015)
8. Kim W, Mungal MG, Cappelli MA. 2010 The role of in situ reforming in plasma enhanced ultra lean premixed methane/air flames. *Combust. Flame* **157**, 374–383. (doi:10.1016/j.combustflame.2009.06.016)
9. Bak MS, Do H, Mungal MG, Cappelli MA. 2012 Plasma-assisted stabilization of laminar premixed methane/air flames around the lean flammability limit. *Combust. Flame* **159**, 3128–3137. (doi:10.1016/j.combustflame.2012.03.023)
10. Nomaguchi T, Koda S. 1989 Spark ignition of methane and methanol in ozonized air. *Proc. Combust. Inst.* **22**, 1677–1682. (doi:10.1016/S0082-0784(89)80180-8)

11. Takita K, Masuya G, Sato T, Ju Y. 1999 Effects of addition of radicals supplied by plasma torch on burning velocity. In *35th AIAA/ASME/SAE/ASEE Joint Propulsion Conf., Los Angeles, CA, 20–24 June 1999*, AIAA paper 1999-2247.
12. Starikovskii AY. 2005 Plasma supported combustion. *Proc. Combust. Inst.* **30**, 2405–2417. (doi:10.1016/j.proci.2004.08.272)
13. Ohisa H, Kimura I, Horisawa H. 1999 Control of soot emission of a turbulent diffusion flame by DC or AC corona discharges. *Combust. Flame* **116**, 653–661. (doi:10.1016/S0010-2180(98)00054-6)
14. Cha MS, Lee SM, Kim KT, Chung SH. 2005 Soot suppression by nonthermal plasma in coflow jet diffusion flames using a dielectric barrier discharge. *Combust. Flame* **141**, 438–447. (doi:10.1016/j.combustflame.2005.02.002)
15. Starikovskiy A, Aleksandrov N. 2013 Plasma-assisted ignition and combustion. *Prog. Energy Comb. Sci.* **39**, 61–110. (doi:10.1016/j.pecs.2012.05.003)
16. Sun W, Uddi M, Won SH, Ombrello T, Carter C, Ju Y. 2012 Kinetic effects of non-equilibrium plasma-assisted methane oxidation on diffusion flame extinction limits. *Combust. Flame* **159**, 221–229. (doi:10.1016/j.combustflame.2011.07.008)
17. Leonov S, Savelkin K, Firsov A, Yarantsev D. 2010 Fuel ignition and flame front stabilization in supersonic flow using electric discharge. *High Temp.* **48**, 896–902. (doi:10.1134/S0018151X10060179)
18. Gluckstein M, Morrison R, Khammash T. 1955 Combustion with ozone-modification of flame speeds: C_2 hydrocarbon-air mixtures. Report no. OSR-TN-55-227, University of Michigan, Ann Arbor, MI, USA.
19. Wang ZH, Yang L, Li B, Li ZS, Sun ZW, Alden M, Cen KF, Konnov AA. 2012 Investigation of combustion enhancement by ozone additive in CH_4/air flames using direct laminar burning velocity measurements and kinetic simulations. *Combust. Flame* **159**, 120–129. (doi:10.1016/j.combustflame.2011.06.017)
20. Halter F, Higelin P, Dagaut P. 2011 Experimental and detailed kinetic modeling study of the effect of ozone on the combustion of methane. *Energy Fuels* **25**, 2909–2916. (doi:10.1021/ef200550m)
21. Vu TM, Won SH, Ombrello T, Cha MS. 2014 Stability enhancement of ozone-assisted laminar premixed Bunsen flames in nitrogen co-flow. *Combust. Flame* **161**, 917–926. (doi:10.1016/j.combustflame.2013.09.023).
22. Ombrello T, Won SH, Ju Y, Williams S. 2010 Flame propagation enhancement by plasma excitation of oxygen. Part I: effects of O_3. *Combust. Flame* **157**, 1906–1915. (doi:10.1016/j.combustflame.2010.02.005)
23. Masurier JB, Foucher F, Dayma G, Dagaut P. 2013 Homogeneous charge compression ignition combustion of primary reference fuels influenced by ozone addition. *Energy Fuels* **27**, 5495–5505. (doi:10.1021/ef401009x)
24. Foucher F, Higelin P, Mounaïm-Rousselle C, Dagaut P. 2013 Influence of ozone on the combustion of *n*-heptane in a HCCI engine. *Proc. Combust. Inst.* **34**, 3005–3012. (doi:10.1016/j.proci.2012.05.042)
25. Schönborn A, Hellier P, Aliev AE, Ladommatos N. 2010 Ignition control of homogeneous-charge compression ignition (HCCI) combustion through adaptation of the fuel molecular structure by reaction with ozone. *Fuel* **89**, 3178–3184. (doi:10.1016/j.fuel.2010.06.005)
26. Batakliev T, Georgiev V, Anachkov M, Rakovsky S, Zaikov GE. 2014 Ozone decomposition. *J. Inform. Intell. Knowl.* **6**, 427–451. (doi:10.2478/intox-2014-0008)
27. Law CK. 2010 *Combustion physics*. Cambridge, UK: Cambridge University Press.
28. Ombrello T, Carter C, Katta V. 2012 Burner platform for sub-atmospheric pressure flame studies. *Combust. Flame* **159**, 2363–2373. (doi:10.1016/j.combustflame.2012.03.010)
29. Malicet J, Daumont D, Charbonner J, Parisse C, Chakir A, Brion J. 1995 Ozone UV spectroscopy. II. Absorption cross-sections and temperature dependence. *J. Atmos. Chem.* **21**, 263–273. (doi:10.1007/BF00696758)
30. PREMIX from the CHEMKIN package. Reaction Design, 6440 Lusk Boulevard, Suite D-205 San Diego, CA 92121. See http://www.reactiondesign.com.
31. Wang H, You X, Joshi AV, Davis SG, Laskin A, Egolfopoulos F, Law CK. 2007 USC Mech Version II. High-Temperature Combustion Reaction Model of H2/CO/C1-C4 Compounds. See http://ignis.usc.edu/USC_Mech_II.htm.

32. Gao X, Zhang Y, Adusumilli S, Seitzman JM, Sun W, Ombrello T, Carter CD. 2015 The effect of ozone addition of flame propagation. In *53rd AIAA Aerospace Sciences Meeting, Kissimmee, FL, 5–9 January 2015*, AIAA paper 2015-0669.
33. Roquemore WM, Katta VR. 1998 Role of flow visualization in the development of UNICORN. *J. Vis.* **2**, 257–272. (doi:10.1007/BF03181442)
34. Katta VR, Goss LP, Roquemore WM. 1994 Effect of nonunity Lewis number and finite-rate chemistry on the dynamics of a hydrogen-air jet diffusion flame. *Combust. Flame* **96**, 60–74. (doi:10.1016/0010-2180(94)90158-9)
35. Katta VR, Goss LP, Roquemore WM. 1994 Numerical investigations of transitional H_2/N_2 jet diffusion flames. *AIAA J.* **32**, 84–94. (doi:10.2514/3.11954)
36. Katta VR, Goss LP, Roquemore WM. 1994 Simulation of vortical structures in a jet diffusion flame. *Int. J. Numer. Methods Heat Fluid Flow* **4**, 413–424. (doi:10.1108/EUM0000000004046)
37. DeMore WB, Sander SP, Golden DM, Hampson RF, Kurylo MJ, Howard CJ, Ravishankara AR, Kolb CE, Molina MJ. 1997 *Chemical kinetics and photochemical data for use in stratospheric modeling*. Jet Propulsion Laboratory Publication 97–4. Pasadena, CA: California Institute of Technology.